REPORT DOCUMENTATION PAGE

Form Approved
OMB No. 0704-0188

Public reporting burden for this collection of information is estimated to average 1 hour per response, including the time for reviewing instructions, searching existing data sources, gathering and maintaining the data needed, and completing and reviewing this collection of information. Send comments regarding this burden estimate or any other aspect of this collection of information, including suggestions for reducing this burden to Department of Defense, Washington Headquarters Services, Directorate for Information Operations and Reports (0704-0188), 1215 Jefferson Davis Highway, Suite 1204, Arlington, VA 22202-4302. Respondents should be aware that notwithstanding any other provision of law, no person shall be subject to any penalty for failing to comply with a collection of information if it does not display a currently valid OMB control number. **PLEASE DO NOT RETURN YOUR FORM TO THE ABOVE ADDRESS.**

1. REPORT DATE *(DD-MM-YYYY)*	**2. REPORT TYPE**	**3. DATES COVERED** *(From - To)*
01-10-2006	Final report	05-15-2005 – 11-14-2005

4. TITLE AND SUBTITLE
Hybrid Molecomputer Using Vapor Phase Assembly

5a. CONTRACT NUMBER
NA

5b. GRANT NUMBER
FA9550-05-1-0340

5c. PROGRAM ELEMENT NUMBER
NA

6. AUTHOR(S)
Reed, Mark A.

5d. PROJECT NUMBER
NA

5e. TASK NUMBER
NA

5f. WORK UNIT NUMBER
NA

7. PERFORMING ORGANIZATION NAME(S) AND ADDRESS(ES)

Yale University
Grant and Contract Admin.
155 Whitney Ave Suite 214
New Haven, CT 06520-8337

8. PERFORMING ORGANIZATION REPORT NUMBER
NA

9. SPONSORING / MONITORING AGENCY NAME(S) AND ADDRESS(ES)
AFOSR
4015 Wilson Blvd
Room 713
Arlington, VA 22203-1954

10. SPONSOR/MONITOR'S ACRONYM(S)
AFOSR

11. SPONSOR/MONITOR'S REPORT NUMBER(S)
AFRL-SR-AR-06-0233

12. DISTRIBUTION / AVAILABILITY STATEMENT
Public distribution/availability

13. SUPPLEMENTARY NOTES

14. ABSTRACT
Current work on molecular electronics relies almost entirely on liquid phase processing. Gas phase processing offers far superior uniformity and reproducibility. The scope of this work was to investigate vapor phase process that will fully integrate the in-situ steps of sample preparation, active organic molecule deposition, and gentle gas-moderated metallic over-coating, which will enable our proposed multi-layer stacked device. The goal of this work is to mate these active molecular gates with a MOS-based post-processing circuit.

15. SUBJECT TERMS
molecular electronics, VPE

16. SECURITY CLASSIFICATION OF:			**17. LIMITATION OF ABSTRACT**	**18. NUMBER OF PAGES**	**19a. NAME OF RESPONSIBLE PERSON**
a. REPORT	**b. ABSTRACT**	**c. THIS PAGE**			Dr. Anne Matsuura
none	none	none	NA		**19b. TELEPHONE NUMBER** *(include area code)* 703-696-6204

Standard Form 298 (Rev. 8-98)
Prescribed by ANSI Std. Z39.18

Objectives

The objectives of this effort are to explore the use of a functionalized semiconductor nanowire matrix with nucleic acid reporters for chem/bio sensors. The milestones were:

- demonstrate unambiguous detection of an analyte in an aqueous environment by gating of a semiconductor nanowire
- demonstrate identification of an analyte using a functionalized nanowire process
- demonstrate nucleotide functionalization of a semiconductor nanowire.
- downselect the specific nanowires and target functionalizations

Status

All milestones listed above were achieved. The program is continuing into Phase II funding. The progress is detailed in the next section

Accomplishments/New Findings

Background

In recent years, investigators have made tremendous strides in demonstrating the basic capabilities of molecular-based electronics. However, this work consists largely of simple circuits, fabricated under carefully controlled laboratory conditions, by extremely well trained investigators. The goal of this program is to develop a hybrid molecular/solid-state circuit configuration that will be fabricated by a more scaleable and production-worthy vapor phase fabrication process. The hybrid approach builds on and combines existing capabilities of molecular and solid-state circuits: The functional unit is a bistable molecular gate consisting of either a stacked negative differential resistive (NDR) or memory molecular device. This device has already been successfully demonstrated. These active molecular gates will then be mated with a MOS-based post-processing circuit to make dense, high-performance cells. This union will be facilitated by new vapor phase deposition process will allow vastly more controlled fabrication of the fully stacked molecular gates upon a MOS-based substrate template.

Current work on molecular electronics relies, almost entirely, on liquid phase processing. Liquid phase processing is simple, it is inexpensive, and it builds upon a large body of experience with self-assembled molecular monolayers (SAMs). We now want to drive molecular circuits to a complexity that will match (and eventually exceed) that of solid-state microelectronics. Early microelectronic processing was also based on the use of liquids. However, as circuit complexity and area increased, liquid-based processing could not deliver the uniformity and reproducibility required for successful fabrication. Thus, virtually all modern semiconductor tools are based on the use of gases. Gas phase processing offers far superior uniformity and reproducibility. Indeed, when surface reactions dominate, it is possible to simultaneously deposit or etch the surfaces of dozens of stacked wafers. More subtly, gases (and ions) allow for very precise and shallow etching. This is essential in the fabrication of a circuit of microprocessor-level complexity: microprocessors cannot be fabricated in a single deposition step. The operation of the device cell, and interconnection of cells, inevitably requires a complex multi-level structure. It is thus essential that the technology allow for repeated reinsertion into deposition systems. For such a sequence of depositions to work, one must be able to clean and prepare underlying structures, in-situ, for the deposition of new materials. Controlled deposition *and* etching are thus essential.

This project is a collaboration between University of Virginia and Yale University. Yale's

responsibility was the fabrication and characterization of molecular devices; UVA had the responsibility of vapor phase molecular deposition. This report focuses on the fabrication and transport data.

Progress and Accomplishments

The suggestion[1] and demonstration[2] of utilizing molecules as the active region of electronic devices has recently generated considerable interest in both the basic transport physics and potential technological applications of "molecular electronics".[3,4] However some reports of molecular mechanisms in electronic devices[5,6] have been shown to be premature and due to filamentary conduction,[7] highlighting the fabrication sensitivity of molecular structures and the need to institute reliable controls and methods to validate true molecular transport.[8] A related problem is the characterization of molecules in the active device structure, including their configuration, bonding, and indeed even their very presence. Here we present results on well-understood molecular assemblies, which exhibit an understood classical transport behavior, and which can be used as a control for eliminating (or understanding) fabrication variables. Utilizing tunneling spectroscopic methods, we present the first unambiguous evidence of the presence of molecules in the junction, and further confirm the charge transport mechanism obtained by standard current-voltage characterizations.

A molecular system whose structure and configuration are sufficiently well-characterized such that it can serve as a standard is the extensively studied alkanethiol ($CH_3(CH_2)_{n-1}SH$) self-assembled monolayer (SAM).[9] This system is useful as a control since properly prepared SAMs form single van der Waals crystals,[9,10] and presents a simple classical metal-insulator-metal (M-I-M) tunnel junction when fabricated between metallic contacts due to the large HOMO-LUMO gap (HOMO: highest occupied molecular orbital, LUMO: lowest unoccupied molecular orbital) of approximately 8 eV.[11-13]

Various surface analytical tools have been utilized to investigate the surface and bulk properties of the alkanethiol SAMs, such as X-ray photoelectron spectroscopy,[14] Fourier transform infrared spectroscopy (FTIR),[15] Raman spectroscopy,[16] scanning tunneling microscopy (STM)[10] etc. For example, studies have shown that the bonding of the thiolate group to the gold surface is strong with a bonding energy of ~ 1.7 eV.[9] STM topography examinations revealed that alkanethiols adopt the commensurate crystalline lattice characterized by a $c(4 \times 2)$ superlattice of a $(\sqrt{3} \times \sqrt{3})R30°$.[10,17] FTIR investigation showed that the orientation of the alkanethiol SAMs on Au(111) surfaces are tilted ~ 30° from the surface normal.[18]

Electronic transport through alkanethiol SAMs have also been characterized by STM,[19,20] conducting atomic force microscopy,[21-24] mercury-drop junctions,[25-28] cross-wire junctions,[29] and electrochemical methods.[30-32] These investigations are exclusively at ambient temperature – clearly useful – but insufficient for an unambiguous claim that the transport mechanism is tunneling (of course expected, assuming that the Fermi levels of the contacts lie within the large HOMO-LUMO gap). However in the absence of temperature-dependent current-voltage (I(V,T)) characteristics, other conduction mechanisms (such as thermionic, hopping, or filamentary conduction) cannot be excluded complicate the analysis, and thus such a claim is premature.

Utilizing a nanometer scale device structure that incorporates alkanethiol SAMs, we demonstrate devices that allow I(V,T) and structure-dependent measurements[33,34] with results that can be compared with accepted theoretical models of M-I-M tunneling. The use of this fabrication approach is not special in any way (other than that we have so far found it to be

successful) – indeed we stress that any successful device fabrication method should yield the results described below if one is characterizing the intrinsic molecular transport properties.

The electronic transport is further investigated with the technique of inelastic electron tunneling spectroscopy (IETS).[34] IETS was developed in the 1960's as a powerful spectroscopic tool to study the vibrational spectrum of organic molecules confined inside metal-oxide-metal junctions.[35-39] In our study IETS is utilized for the purpose of molecule identification, chemical bonding and conduction mechanism investigations of the "control" SAMs. The exclusive presence of well-known vibrational modes of the alkanes used are direct evidence of the molecules in the device structure, something that has to date only been inferred (with good reason, but nonetheless not unambiguously). The vibrational modes, exclusively identified as alkanes (as well as contact modes) are difficult to interpret in any other way other than as components in the active region of the device. The inelastic tunneling spectra also demonstrate that electronic tunneling occurs through the molecules, confirming the conduction mechanism obtained by I(V,T) characterizations. The specific spectral lines also yield intrinsic linewidths that may give insight into molecular conformation, and may prove to be a powerful tool in future molecular device characterization.

Electronic transport measurements on alkanethiol SAMs were performed using a device structure similar to one reported previously.[33,34,40-42] In this device, as illustrated in Figure 1(a) (not drawn to scale in the relative thickness), a number of molecules (~ several thousands) are sandwiched between two metallic contacts. This technique provides a stable device structure and makes cryogenic measurements possible. The device fabrication starts with a high resistivity silicon wafer with low stress Si_3N_4 film deposited on both sides by low pressure chemical vapor deposition (LPCVD). By standard photolithography processing, a suspended Si_3N_4 membrane (size of 40 μm × 40 μm and thickness of ~ 70 nm) is fabricated on the topside of the wafer. Subsequent e-beam lithography and reactive ion etching creates a single pore with a diameter of tens of nanometers through the membrane. As the next step, 150 nm gold is thermally evaporated onto the topside of the wafer to fill the pore and form one of the metallic contacts.

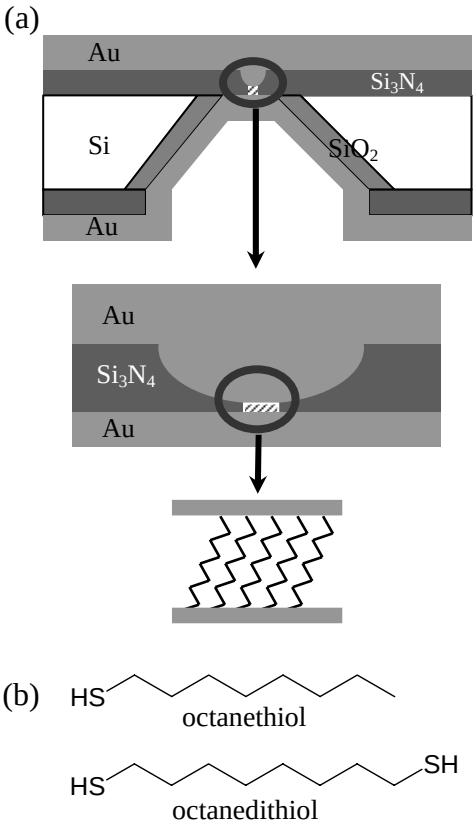

Figure 1. Schematics of a nanometer scale device used in this study (not drawn to scale in the relative thickness). (a) Top schematic is the cross section of a silicon wafer with a nanometer scale pore etched through a suspended silicon nitride membrane. Middle and bottom schematics show a Au/SAM/Au junction formed in the pore area. (b) The structures of octanethiol and octanedithiol are shown as examples.

The device is then transferred into a molecular solution to deposit the SAM layer. For our experiments, a ~ 5 mM alkanethiol solution is prepared by adding ~ 10 μL alkanethiols into 10 mL ethanol.[43] The deposition is done in solution for 24 hours inside a nitrogen filled glove box

with an oxygen level of less than 100 ppm. Three alkanemonothiol molecules of different molecular lengths–octanethiol [$CH_3(CH_2)_7SH$; denoted as C8, for the number of alkyl units], dodecanethiol [$CH_3(CH_2)_{11}SH$, denoted as C12], and hexadecanethiol [$CH_3(CH_2)_{15}SH$, denoted as C16] and one alkanedithiol molecule–octanedithiol [$HS(CH_2)_8SH$, denoted as C8-dithiol] were used to form the active molecular components.[43] As representative examples, the chemical structures of octanethiol and octanedithiol are shown in Figure 1(b).

In order to statistically determine the pore size, test patterns (arrays of pores) were created under similar fabrication conditions. Figure 2 shows a scanning electron microscope (SEM) image of such test pattern arrays. This indirect measurement of device size is done since SEM examination of the actual device can cause hydrocarbon contamination of the device and subsequent contamination of the monolayer. From regression analysis of 298 pores, the device sizes of the C8, C12, C16, and C8-dithiol samples are determined as 50 ± 8, 45 ± 2, 45 ± 2, and 51 ± 5 nm in diameters, respectively. A more ideal (less parasitic) C8 sample supercedes that of previous reports,[33] and derived parameters from the two data sets agree to within a standard error. We will use these device areas as the effective contact areas. Although one could postulate that the actual area of metal that contacts the molecules may be different, there is little reason to propose it would be different as a function of length over the range of alkanethiols used, and at most would be a constant systematic error.

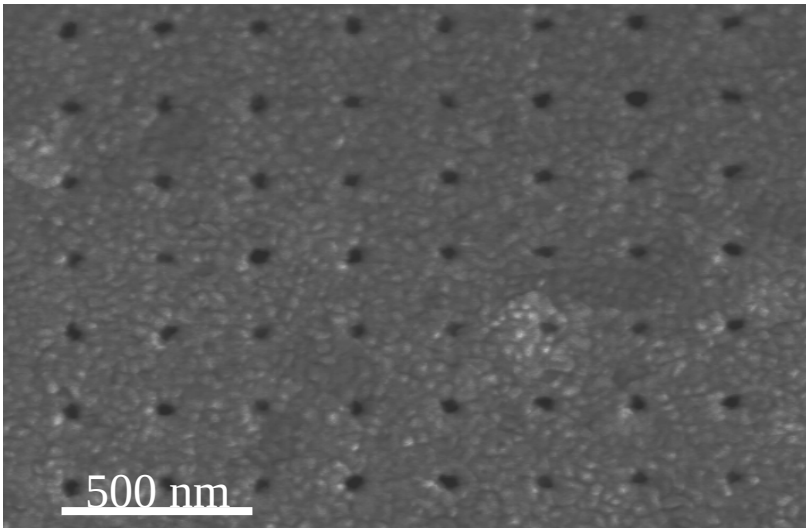

Figure 2. A scanning electron microscope image of a representative array of pores used to calibrate device size. The scale bar is 500 nm.

The sample is then transferred in ambient conditions to an evaporator that has a cooling stage to deposit the opposing Au contact. During the thermal evaporation (under the pressure of ~ 10^{-8} Torr), liquid nitrogen is kept flowing through the cooling stage in order to avoid thermal damage to the molecular layer.[33,44] This technique reduces the kinetic energy of evaporated Au atoms at the surface of the monolayer, thus preventing Au atoms from punching through the monolayer. For the same reason the evaporation rate is kept very low. For the first 10 nm gold evaporated, the rate is less than 0.1 Å/s. Then the rate is increased slowly to 0.5 Å/s for the rest of the evaporation and a total of 200 nm gold is deposited to form the contact.

The device is subsequently packaged and loaded into a low temperature cryostat. The sample temperature is varied from 300 to 4.2 K by flowing cryogen vapor onto the sample (and thermometer) using a closed loop temperature controller. Two-terminal dc I(V) measurements are performed using a semiconductor parameter analyzer. Inelastic electron tunneling spectra are obtained via a standard lock-in second harmonic measurement technique.[35,36] A synthesized function generator is used to provide both the modulation and the lock-in reference signal. The second harmonic signal (proportional to d^2I/dV^2) is directly measured using a lock-in amplifier,

which is checked to be consistent with a numerical derivative of the first harmonic signal (proportional to dI/dV). Various modulation amplitudes and frequencies are utilized to obtain the spectra. The ac modulation is added to a dc bias using operational amplifier-based custom circuitry.[45]

In Table 1, possible conduction mechanisms are listed with their characteristic current, temperature- and voltage-dependencies[46] (We do not discuss filamentary tunneling mechanisms, which are easier to categorize[47]). Based on whether thermal activation is involved, the conduction mechanisms fall into two distinct categories: (i) thermionic or hopping conduction which has temperature-dependent I(V) behavior and (ii) direct tunneling or Fowler-Nordheim tunneling which does not have temperature-dependent I(V) behavior. For example, thermionic and hopping conductions have been observed for 4-thioacetylbiphenyl SAMs[40] and 1,4-phenelyene diisocyanide SAMs.[41b] On the other hand, the conduction mechanism is expected to be tunneling when the Fermi levels of contacts lie within the large HOMO-LUMO gap for short length molecule, as for the case of alkanethiol molecular system.[11-13] Previous work on Langmuir-Blodgett alkane monolayers[48] exhibited a significant impurity-dominated transport component, complicating the analysis. I(V) measurements on self-assembled alkanethiol monolayers have also been reported;[19-29,49] however all of these measurements were performed at fixed temperature (300 K) which is insufficient to prove tunneling as the dominant mechanism.

TABLE 1. Possible conduction mechanisms. Adapted from Ref. 46.

Conduction Mechanism	Characteristic Behavior	Temperature Dependence	Voltage Dependence
Direct Tunneling*	$J \sim V \exp(-\frac{2d}{\hbar}\sqrt{2m\Phi})$	none	$J \sim V$
Fowler-Nordheim Tunneling	$J \sim V^2 \exp(-\frac{4d\sqrt{2m}\,\Phi^{3/2}}{3q\hbar V})$	none	$\ln(\frac{J}{V^2}) \sim \frac{1}{V}$
Thermionic Emission	$J \sim T^2 \exp(-\frac{\Phi - q\sqrt{qV/4\pi\varepsilon d}}{kT})$	$\ln(\frac{J}{T^2}) \sim \frac{1}{T}$	$\ln(J) \sim V^{\frac{1}{2}}$
Hopping Conduction	$J \sim V \exp(-\frac{\Phi}{kT})$	$\ln(\frac{J}{V}) \sim \frac{1}{T}$	$J \sim V$

* This characteristic of direct tunneling is valid for the low bias regime [see Eq. (3a)].

To describe the transport through a molecular system having HOMO and LUMO energy levels, one of the applicable models is the Franz two-band model.[50-53] This model provides a non-parabolic energy-momentum E(k) dispersion relationship by considering the contributions of both the HOMO and LUMO energy levels:[50]

$$k^2 = \frac{2m^*}{\hbar^2} E\,(1+\frac{E}{E_g}) \qquad (1)$$

where k is the imaginary part of wave vector of electrons, m* is the electron effective mass, h (= $2\pi\hbar$) is Planck's constant, E is the electron energy, and E_g is the HOMO-LUMO energy gap. From this non-parabolic E(k) relationship, the effective mass of the electron tunneling through the SAM can be deduced by knowing the barrier height of the metal-SAM-metal junction.

When the Fermi level of the metal is aligned close enough to one energy level (either HOMO or LUMO), the effect of the other distant energy level on the tunneling transport is negligible, and the widely used Simmons model[54] is an excellent approximation.[55] Simmons model expressed the tunneling current density through a barrier in the tunneling regime of $V < \Phi_B/e$ as[25,54]

$$J = \left(\frac{e}{4\pi^2\hbar\, d^2}\right)\left\{\left(\Phi_B - \frac{eV}{2}\right)\exp\left[-\frac{2(2m)^{1/2}}{\hbar}\alpha\left(\Phi_B - \frac{eV}{2}\right)^{1/2} d\right]\right. \qquad (2)$$
$$\left. - \left(\Phi_B + \frac{eV}{2}\right)\exp\left[-\frac{2(2m)^{1/2}}{\hbar}\alpha\left(\Phi_B + \frac{eV}{2}\right)^{1/2} d\right]\right\}$$

where m is the electron mass, d is the barrier width, Φ_B is the barrier height, and V is the applied bias. For molecular systems, the Simmons model has been modified with a parameter α.[25,33] α is a unitless adjustable parameter that is introduced to provide either a way of applying the tunneling model of a rectangular barrier to tunneling through a nonrectangular barrier,[25] or an adjustment to account for the effective mass (m*) of the tunneling electrons through a rectangular barrier,[25,33,53,56] or both. $\alpha = 1$ corresponds to the case for a rectangular barrier and bare electron mass. By fitting individual I(V) data using Eq. (2), Φ_B and α values can be obtained.

Eq. (2) can be approximated in two limits: low bias and high bias as compared with the barrier height Φ_B. For the low bias range, Eq. (2) can be approximated as[54]

$$J \approx \left(\frac{(2m\Phi_B)^{1/2} e^2 \alpha}{h^2 d}\right) V \exp\left[-\frac{2(2m)^{1/2}}{\hbar}\alpha(\Phi_B)^{1/2} d\right] \qquad (3a)$$

To determine the high bias limit, we compare the relative magnitudes of the first and second exponential terms in Eq. (2). At high bias, the first term is dominant and thus the current density can be approximated as

$$J \approx \left(\frac{e}{4\pi^2 \hbar\, d^2}\right)\left(\Phi_B - \frac{eV}{2}\right)\exp\left[-\frac{2(2m)^{1/2}}{\hbar}\alpha\left(\Phi_B - \frac{eV}{2}\right)^{1/2} d\right] \qquad (3b)$$

The tunneling currents in both bias regimes are exponentially dependent on the barrier width d. In the low bias regime the tunneling current density is $J \propto \frac{1}{d}\exp(-\beta_0 d)$, where β_0 is bias-independent decay coefficient:

$$\beta_0 = \frac{2(2m)^{1/2}}{\hbar}\alpha\left(\Phi_B\right)^{1/2} \qquad (4a)$$

while in the high bias regime, $J \propto \frac{1}{d^2}\exp(-\beta_V d)$, where β_v is bias-dependent decay coefficient:

$$\beta_V = \frac{2(2m)^{1/2}}{\hbar}\alpha\left(\Phi_B - \frac{eV}{2}\right)^{1/2} = \beta_0\left(1 - \frac{eV}{2\Phi_B}\right)^{1/2} \qquad (4b)$$

At high bias β_V decreases as bias increases, which results from barrier lowering effect due to the applied bias.

In order to determine the conduction mechanism of self-assembled alkanethiol molecular systems I(V) measurements in a sufficiently wide temperature range (300 to 80 K) and resolution (10 K) were performed. Figure 3(a) shows a representative I(V,T) characteristic of dodecanethiol (C12) measured with the device structure as shown in Figure 1(a). Positive bias corresponds to electrons injected from the physisorbed Au contact [bottom contact in Figure 1(a)] into the molecules. By using the contact area of 45 ± 2 nm in diameter determined from SEM study, a current density of 1,500 ± 200 A/cm^2 at 1.0 Volt is determined. No significant temperature dependence of the characteristics (from V = 0 to 1.0 Volt) is observed over the range from 300 to 80 K. An Arrhenius plot (ln(I) versus 1/T) of this is shown in Figure 3(b), exhibiting little temperature dependence in the slopes of ln(I) versus 1/T at different bias and thus indicating the absence of thermal activation. Therefore, we conclude that the conduction mechanism through alkanethiol is tunneling contingent on demonstrating a correct molecular length dependence. The tunneling through alkanethiol SAMs has been assumed as "through-bond" tunneling, i.e., along the tilted molecular chains between the metal contacts.[22,23,32,57] Based on the applied bias as compared with the barrier height (Φ_B), the tunneling through a SAM layer can be categorized into either direct ($V < \Phi_B/e$) or Fowler-Nordheim ($V > \Phi_B/e$) tunneling. These two tunneling mechanisms can be distinguished due to their distinct voltage dependencies (see Table 1). Analysis of ln(I/V^2) versus 1/V [in Figure 3(c)] shows no significant voltage dependence, indicating no obvious Fowler-Nordheim transport behavior in this bias range (0 to 1.0 Volt) and thus determining that the barrier height is larger than the applied bias, i.e., $\Phi_B > 1.0$ eV. This study is restricted to applied biases ≤ 1.0 Volt and the transition from direct to Fowler-Nordheim tunneling requires higher bias.

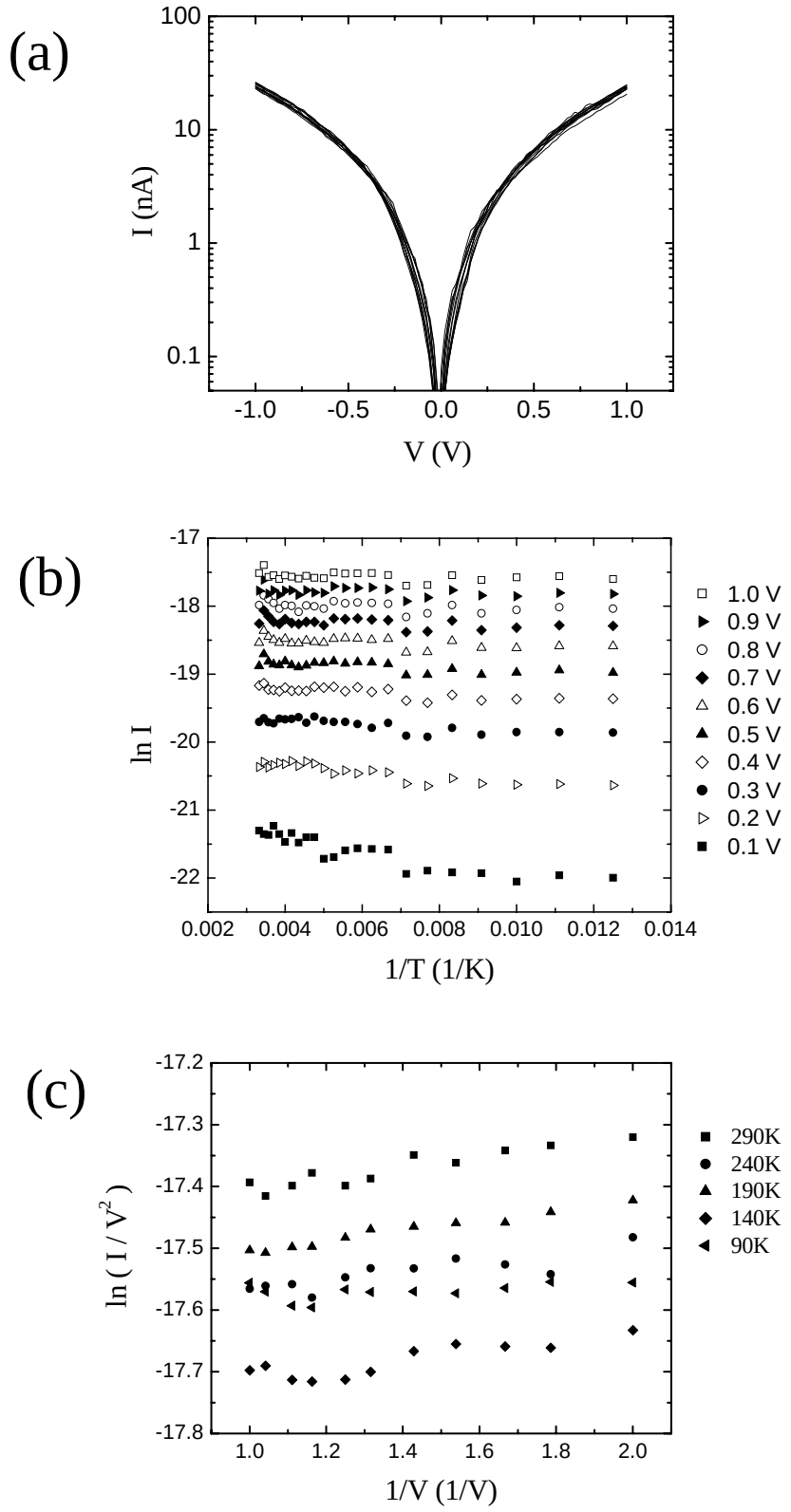

Figure 3. (a) Temperature-dependent I(V) characteristics of dodecanethiol (C12). I(V) data at temperatures from 300 to 80 K with 20 K steps are plotted on a log scale. (b) Arrhenius plot generated from the I(V) data in (a), at voltages from 0.1 to 1.0 Volt with 0.1 Volt steps. (c) Plot of $\ln(I/V^2)$ versus 1/V at selected temperatures.

The importance of variable temperature measurements to validate tunneling is demonstrated in Figure 4. Here the I(V) of an octanethiol (C8) device is shown (Figure 4(a)), whose I(V) shape looks very similar to Figure 3 (i.e., direct tunneling), and indeed can be fit to a Simmons model. However, further I(V,T) measurements display an obvious temperature dependence (Figure 4(b)), which can be fit well to a hopping conduction model (Table 1) with a well-defined activation energy of 190 meV (Figure 4(c)). This and other similar impurity-mediated transport phenomena (such as Coulomb blockade) are observed in a subset of devices and is indicative of the unintentional incorporation of a trap or defect level in those devices. This study instead focuses on devices which do not show any defect-mediated transport and probes the intrinsic behavior of the molecular layer.

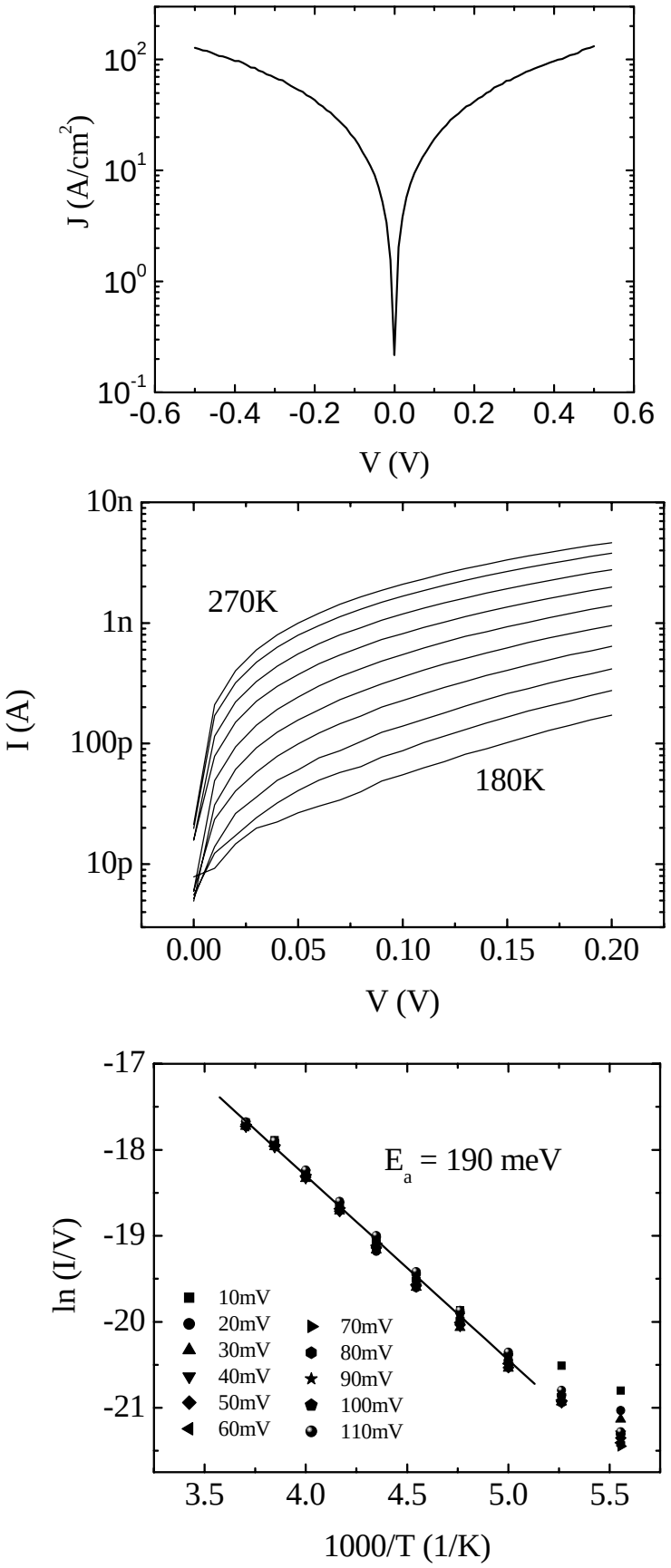

Figure 4. (a) I(V) characteristics of an octanethiol (C8) device at 270K. (b) Temperature dependence of the device from 270K to 180K (in 10K increments). (c) Plot of ln(I/V) versus 1/T at various voltages. The activated behavior is bias voltage independent, thus the behavior is hopping (in this device) due to incorporation of a defect of energy 190 meV. This class of device is not suitable for investigation of the intrinsic transport mechanism in the SAM as it is dominated by a defect.

Having established tunneling as the conduction mechanism in a device, we will now obtain the barrier height by comparing experimental I(V) data with theoretical calculations from tunneling models.

From the modified Simmons model [Eq. (2)] by adjusting two parameters Φ_B and α, a nonlinear least squares fitting can be performed to fit the measured C12 I(V) data (calculation assuming $\alpha = 1$ has been previously shown not to fit I(V) data well for some alkanethiol measurements at fixed temperature (300 K)).[25] By using a device size of 45 nm in diameter, the best fitting parameters (minimizing χ^2) for the room temperature C12 I(V) data were found to be $\Phi_B = 1.42 \pm 0.04$ eV and $\alpha = 0.65 \pm 0.01$, where the error ranges of Φ_B and α are dominated by potential device size fluctuations of 2 nm. Likewise,

data sets were obtained and fittings were done for octanethiol (C8) and hexadecanethiol (C16), which yielded values {$\Phi_B = 1.83 \pm 0.10$ eV and $\alpha = 0.61 \pm 0.01$} and {$\Phi_B = 1.40 \pm 0.03$ eV, $\alpha = 0.68 \pm 0.01$}, respectively.

Using $\Phi_B = 1.42$ eV and $\alpha = 0.65$, a calculated I(V) for C12 is plotted as a solid curve in a linear scale [Figure 5(a)] and in a semi-log scale [Figure 5(b)]. A calculated I(V) for $\alpha = 1$ and $\Phi_B = 0.65$ eV (which gives the best fit at low bias range) is shown as the dashed curve in the same figure, illustrating that with $\alpha = 1$ only limited regions of the I(V) can be fit (specifically here, for V < 0.3 Volt). For the case of a rectangular barrier, the α parameter fit presented above corresponds to an effective mass m* (= α^2 m) of 0.42 m.

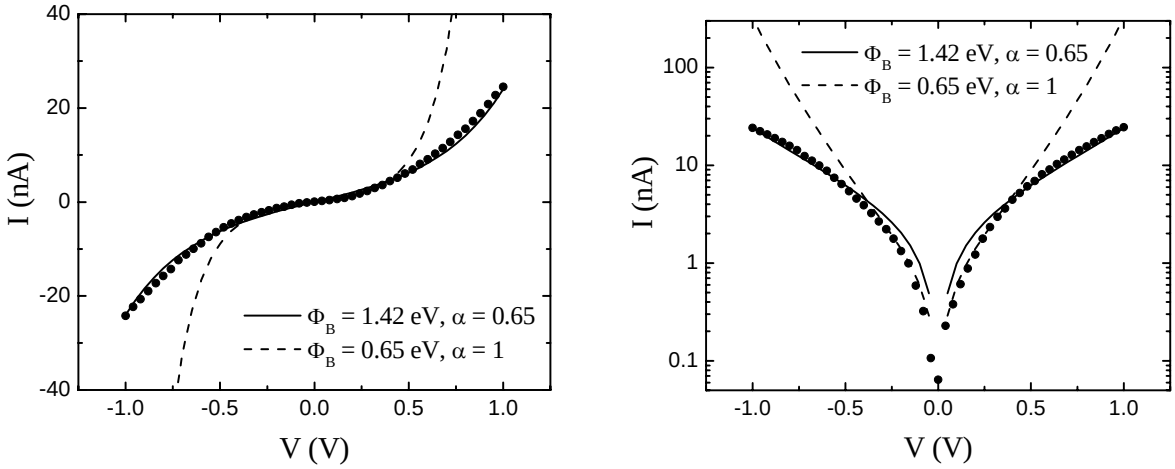

Figure 5. Measured C12 I(V) data (circular symbols) is compared with calculation (solid curve) using the optimum fitting parameters of $\Phi_B = 1.42$ eV and $\alpha = 0.65$. The calculated I(V) from a simple rectangular model ($\alpha = 1$) with $\Phi_B = 0.65$ eV is also shown as the dashed curve. Current is plotted (a) on linear scale and (b) on log scale.

In order to investigate the dependency of the Simmons model fitting on Φ_B and α, a fitting minimization analysis was undertaken on the individual Φ_B and α values as well as their product form of $\alpha\Phi_B^{1/2}$ in Eq. (4a). $\Delta(\Phi_B, \alpha) = (\Sigma \mid I_{exp,V} - I_{cal,V} \mid^2)^{1/2}$ was calculated and plotted where $I_{exp,V}$ is the experimental current-voltage values and $I_{cal,V}$ is calculated using Eq. (2). 7,500 different {Φ_B, α} pairs were used in the fittings with Φ_B ranging from 1.0 to 2.5 eV (0.01 eV increment) and α from 0.5 to 1.0 (0.01 increment). Figure 6(a) is a representative contour plot of $\Delta(\Phi_B, \alpha)$ versus Φ_B and α values generated for the C12 I(V) data where darker regions correspond to smaller $\Delta(\Phi_B, \alpha)$ and various shades represent half order of magnitude $\Delta(\Phi_B, \alpha)$ steps. The darker regions represent better fits of Eq. (2) to the measured I(V) data. In the inset in Figure 6(a) one can see there is a range of possible Φ_B and α values yielding minimum fitting parameters. Although the tunneling parameters determined from the previous Simmons tunneling fitting {$\Phi_B = 1.42$ eV and $\alpha = 0.65$} lie within this minimum region in this figure, there is a distribution of other possible values.

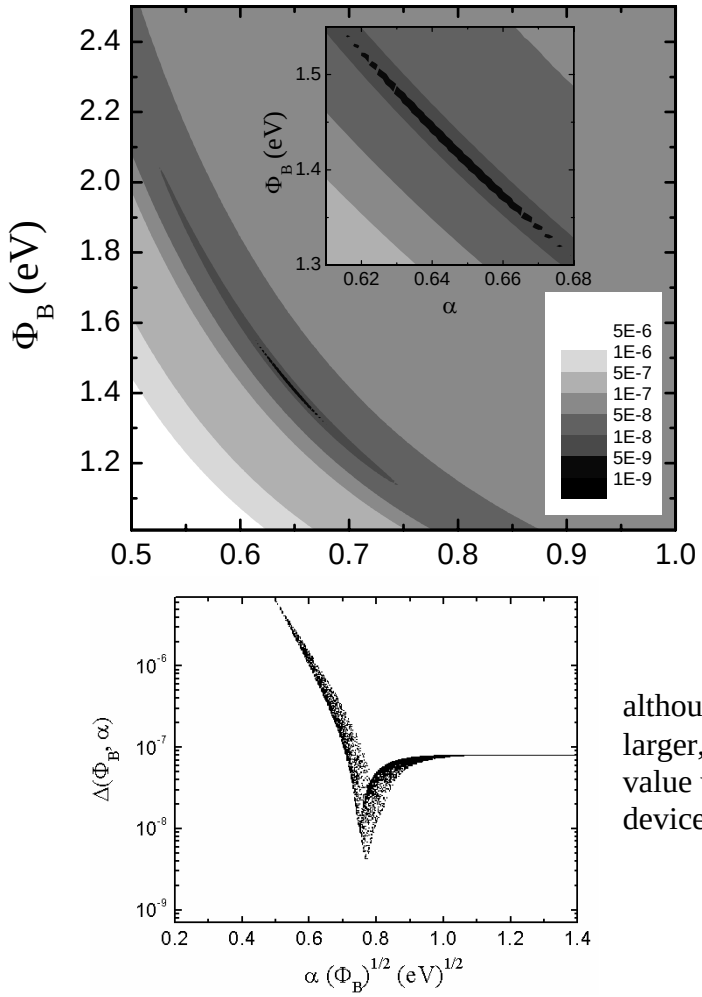

Figure 6. (a) Contour plot of $\Delta(\Phi_B, \alpha)$ values for C12 nanopore device as a function of Φ_B and α, where the darker region corresponds to a better fitting. Inset shows detailed minimization fitting regions. (b) A plot of $\Delta(\Phi_B, \alpha)$ as a function of $\alpha\ \Phi_B^{1/2}$.

A plot of $\Delta(\Phi_B, \alpha)$ versus $\alpha\Phi_B^{1/2}$ for the same device reveals a more pronounced dependence, and is shown in Figure 6(b). This plot indicates the fitting to the Simmons model sharply depends on the product of $\alpha\Phi_B^{1/2}$. For this plot the $\Delta(\Phi_B, \alpha)$ is minimized at $\alpha\Phi_B^{1/2}$ of 0.77 $(eV)^{1/2}$ corresponding to a β_0 value of 0.79 $Å^{-1}$ from Eq. (4a). The C8 and C16 devices showed similar results, indicating the Simmons tunneling model has a strong $\alpha\Phi_B^{1/2}$ dependence. For the C8 device, although Φ_B obtained from the fitting is a little larger, combined α and Φ_B gives a similar β_0 value within the error range as the C12 and C16 devices (Table 2).

TABLE 2. Summary of alkanethiol tunneling parameters in this study

Molecules	J at 1 V (A/cm2)	Φ_B (eV)	α	m* (m)	β_0 ($Å^{-1}$)*
C8	31,000 ± 10,000	1.83 ± 0.10	0.61 ± 0.01	0.37	0.85 ± 0.04
C12	1,500 ± 200	1.42 ± 0.04	0.65 ± 0.01	0.42	0.79 ± 0.02
C16	23 ± 2	1.40 ± 0.03	0.68 ± 0.01	0.46	0.82 ± 0.02
C8-dithiol	93,000 ± 18,000	1.20 ± 0.03	0.59 ± 0.01	0.35	0.66 ± 0.02

* β_0 values were calculated using Eq. (4a).

Three alkanethiols of different molecular length, C8, C12, and C16 were investigated to study length-dependent tunneling behavior. Figure 7 is a semi-log plot of tunneling current densities multiplied by molecular length (Jd at low bias and Jd^2 at high bias) as a function of the molecular length for these alkanethiols. The molecular lengths used in this plot are 13.3, 18.2, and 23.2 Å for C8, C12, and C16, respectively. Each molecular length was determined by adding an Au-thiol bonding length to the length of molecule[22]. Note that these lengths assume through-bond tunneling.[22,23,32,57] The high and low bias regimes are defined somewhat arbitrarily by comparing the relative magnitudes of the first and second exponential terms in Eq. (2). Using Φ_B = 1.42 eV and α = 0.65 obtained from nonlinear least squares fitting of the C12 I(V) data, the second term becomes less than ~ 10 % of the first term at ~ 0.5 Volt that is chosen as the boundary of low and high bias ranges.

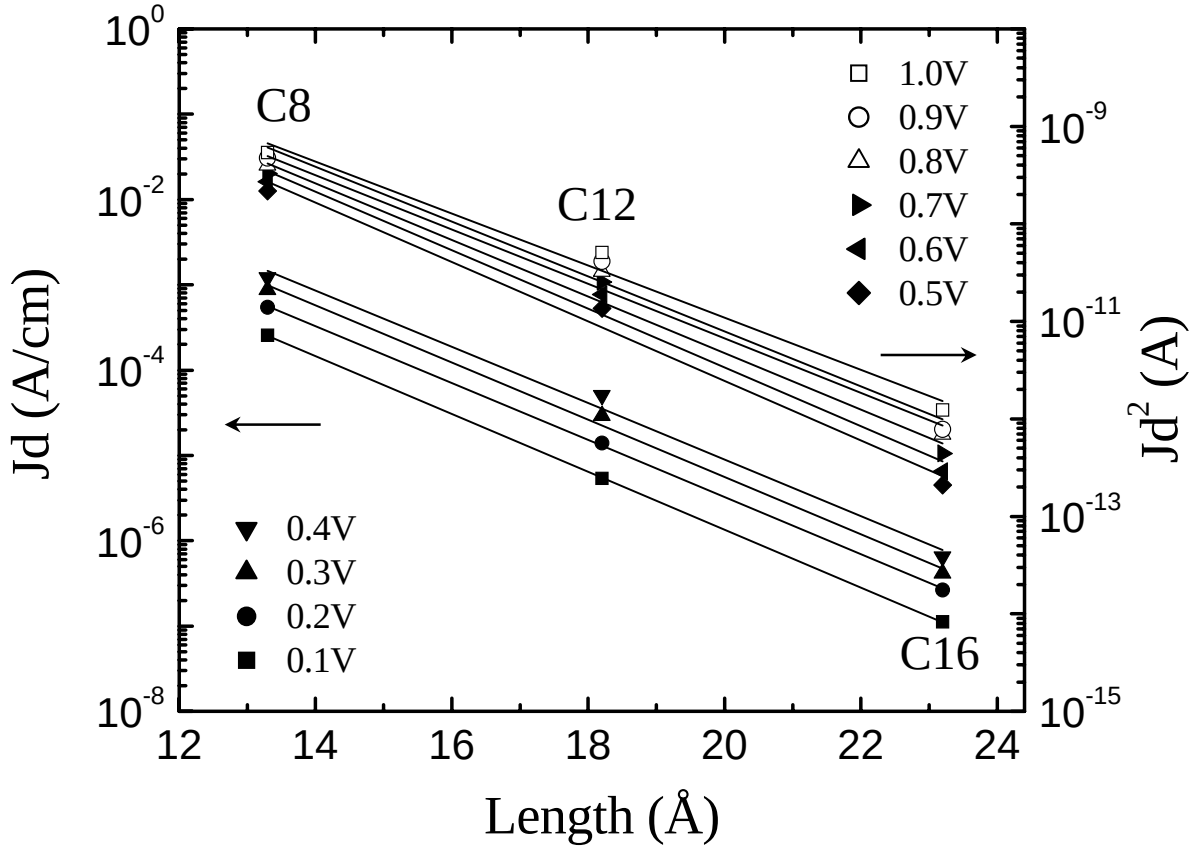

Figure 7. Log plot of tunneling current densities multiplied by molecular length d at low bias and by d^2 at high bias (symbols) versus molecular lengths. The lines through the data points are linear fittings.

As seen in Figure 7, the tunneling current shows exponential dependence on molecular length, which is consistent with the Simmons tunneling model [Eq. (3)]. The β values can be determined from the slope at each bias and are plotted in Figure 8. The error bar of an individual

β value in this plot was obtained by considering both the device size uncertainties and the linear fitting errors.

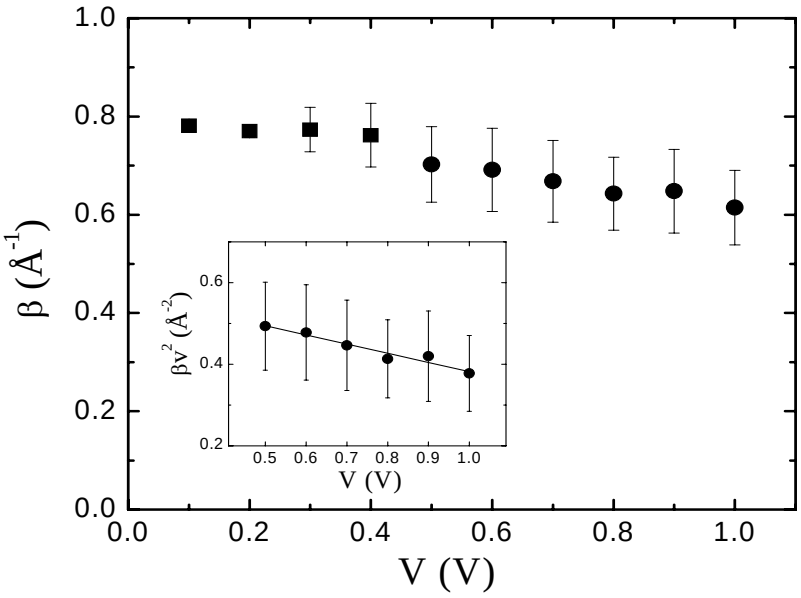

Figure 8. Plot of β versus bias in the low bias range (square symbols) and high bias ranges (circular symbols). The inset shows a plot of β^2_V versus bias with a linear fitting.

The determined β values are almost independent of bias in the low bias range (V < ~ 0.5 V), and an average β of 0.77 ± 0.06 Å^{-1} in this region (from 0 to 0.5 V) can be calculated from Figure 8. Table 3 is a summary of previously reported alkanethiol transport parameters obtained by different techniques. The current densities (J) listed in Table 3 are for C12 monothiol or dithiol devices at 1 V, which are extrapolated from published results of other length alkane molecules. The large variation of J of these reports can be attributed to the uncertainties in device contact geometry and junction area, as well as complicating inelastic or defect contributions. The β value (0.77 ± 0.06 Å^{-1} ≈ 0.96 ± 0.08 per methylene) for alkanethiols reported here is comparable to previously reported values as summarized in Table 3. This β value agrees with the value of 0.79 Å^{-1} (β_0) calculated via Eq. (4a) from fitting individual I(V) characteristic of the C12 device. The calculated β_0 of C8 and C16 devices also have similar values, as summarized in Table 2.

TABLE 3. Summary of alkanethiol tunneling characteristic parameters

Junction	β (Å^{-1})	J (A/cm^2) at 1 V	Φ_B (eV)	Technique	Ref.
(bilayer) monothiol	0.87±0.1	25-200[a)]	2.1[e)]	Hg-junction	25
(bilayer) monothiol	0.71±0.08	0.7-3.5[a)]		Hg-junction	27
monothiol	0.79±0.01	1500±200[b)]	1.4[e)]	Solid M-I-M	33
monothiol	1.2			STM	19
dithiol	0.8±0.08	3.7-5 × 10^5 [c)]	5 ± 2[f)]	STM	20
monothiol	0.73-0.95	1100-1900[d)]	2.2[e)]	CAFM	21
monothiol	0.64-0.8	10-50[d)]	2.3[e)]	CAFM	23
dithiol	0.46±0.02	3-6 × 10^5 [c)]	1.3-1.5[e)]	CAFM	24

monothiol	1.37±0.03		1.8[f)]	Tuning fork AFM	49
monothiol	0.97±0.04			Electrochemical	30
monothiol	0.85			Electrochemical	31
monothiol	0.91±0.08			Electrochemical	32
monothiol	0.76	2×10^4 (at 0.1 V)[c)]	1.3-3.4[g)]	Theory	58
monothiol	0.76			Theory	59
monothiol	0.79			Theory	56

Note:

Some decay coefficients β were converted into the unit of $Å^{-1}$ from the unit of per methylene.

The junction areas were estimated by optical microscope[a)], SEM[b)], assuming single molecule[c)], and Hertzian contact theory[d)].

Current densities (J) for C12 monothiol or dithiol at 1 V are extrapolated from published results for other length molecules by using conductance $\propto \exp(-\beta d)$ relationship.

Barrier height Φ_B values were obtained from Simmons equation[e)], bias-dependence of β[f)], and a theoretical calculation[g)].

According to Eq. (4b), β^2_V depends on bias V linearly in the high bias range. The inset in Figure 8 is a plot of β^2_V versus V in this range (0.5 to 1.0 Volt) along with linear fitting of the data. From this fitting, $\Phi_B = 1.35 \pm 0.20$ eV and $\alpha = 0.66 \pm 0.04$ were obtained from the intercept and the slope, respectively, consistent with the values {$\Phi_B = 1.42$ eV and $\alpha = 0.65$} obtained from the nonlinear least squares fitting in the previous section.

β values for alkanethiols obtained by various experimental techniques have previously been reported and are summarized in Table 3.[19-33,49] In order to compare with these reported β values, we also performed length-dependent analysis on our experimental data according to the generally used equation:[20-28,33]

$$G = G_0 \exp(-\beta d) \qquad (5)$$

This gives a β value from 0.84 to 0.73 $Å^{-1}$ in the bias range from 0.1 to 1.0 volt, which is comparable to results reported previously. For example, Holmlin, *et. al*, reported a β value of 0.87 $Å^{-1}$ by mercury drop experiments,[25] and Wold, *et. al*, have reported β of 0.94 $Å^{-1}$ and Cui, *et. al*, reported β of 0.64 $Å^{-1}$ for various alkanethiols by using a conducting atomic force microscope technique.[21,23] These reported β were treated as bias-independent quantities, contrary to the results reported here and that observed in a slightly different alkane system (ligand-encapsulated nanoparticle/alkane-dithiol molecules).[24] We also caution against the use of parameters that have not been checked with a temperature-dependent analysis, since small non-tunneling components can dramatically affect derived values of β.

We have analyzed our experimental data using a Franz two-band model.[50-53] Since there is no reliable experimental data on the Fermi level alignment in these metal-SAM-metal systems, Φ_B and m* are treated as adjustable parameters. We performed a least squares fit on our data with the Franz non-parabolic E(k) relationship [Eq. (1)] using an alkanethiol HOMO-LUMO gap of 8 eV.[12,13] Figure 9 shows the resultant E(k) relationship and the corresponding energy band diagrams. The zero of energy in this plot was chosen as the LUMO energy. The best fitting

parameters obtained by minimizing χ^2 were $\Phi_B = 1.49 \pm 0.51$ eV and $m^* = 0.43 \pm 0.15$ m, where the error ranges of Φ_B and m^* are dominated by the error fluctuations of β [$k^2 = -(\beta/2)^2$]. Both electron tunneling near the LUMO and hole tunneling near the HOMO can be described by these parameters. $\Phi_B = 1.49$ eV indicates that the Fermi level is aligned close to one energy level in either case, therefore the Simmons model is a valid approximation. The Φ_B and m^* values obtained here are in reasonable agreement with the previous results obtained from the Simmons model.

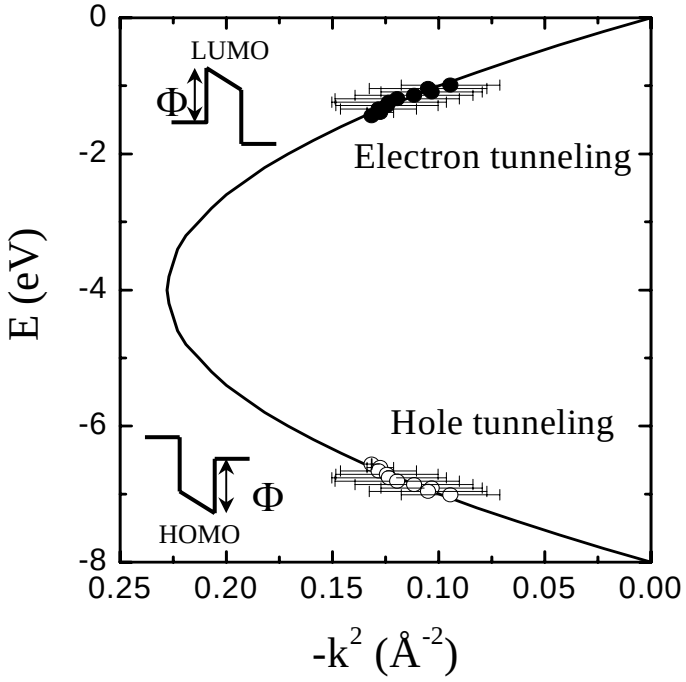

Figure 9. E(k) relationship (symbols) generated from the length-dependent measurement data for alkanethiols. Solid and open symbols correspond to electron and hole tunneling, respectively. The insets show the corresponding energy band diagrams. The solid curve is the Franz two-band expression for $m^* = 0.43$ m.

Electronic transport through alkanethiol SAMs is further investigated with the technique of inelastic electron tunneling spectroscopy,[34] such as the works of 1966 by Jaklevic and Lambe who studied the conductance of a tunnel junctions with encased organic molecules.[35] Since then it has become a powerful spectroscopic tool for chemical identification, chemical bonding investigation, and surface chemistry and physics studies.[38] In an inelastic tunneling process the electron loses energy to a localized vibrational mode with a frequency ν when the applied bias satisfies the condition of $eV = h\nu$. As a result, an additional tunneling channel is opened for the electron, resulting in an increase in the total current at the applied bias corresponding to the vibrational mode energy.[37] Typically only a small fraction of tunneling electrons are involved in the inelastic tunneling process (determined by the electron – vibronic mode coupling coefficient), resulting in a small conductance change, which is commonly measured in the second harmonics of a phase-sensitive detector that yields the characteristic frequencies of the corresponding vibrational modes as well as other information.[36-38]

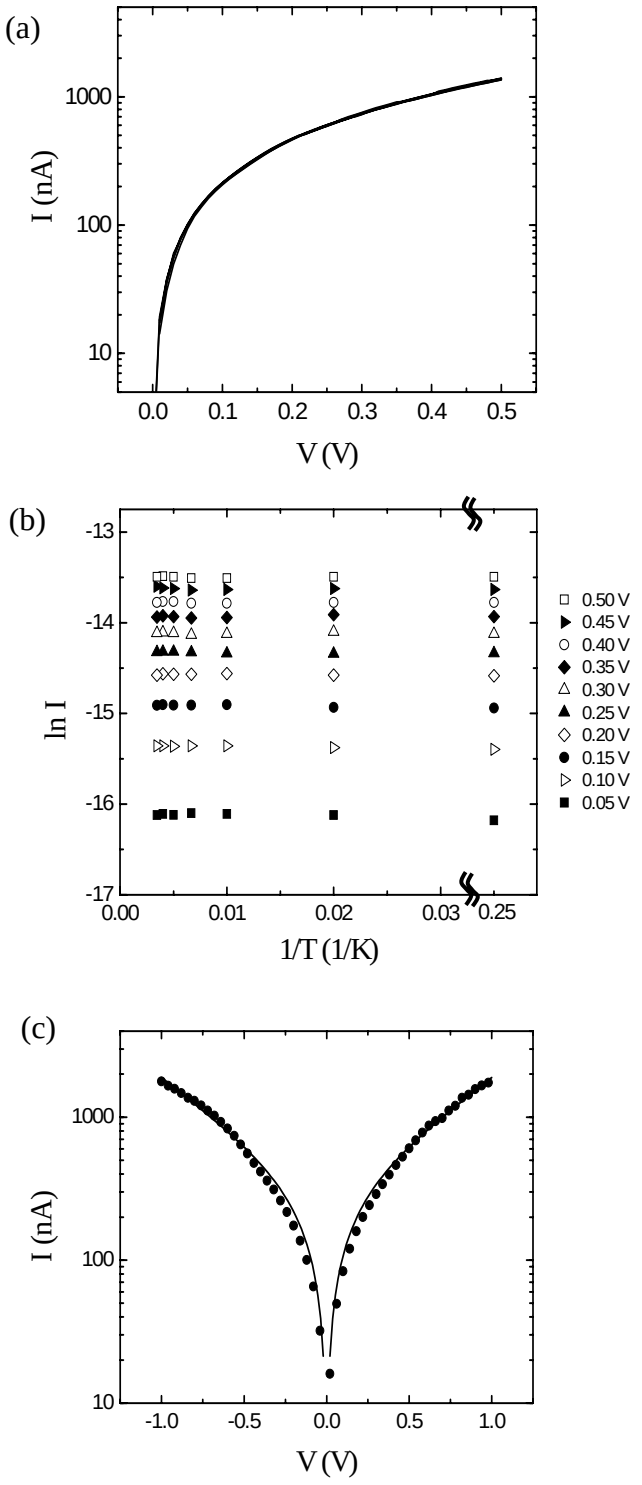

I(V,T) measurements and additional IETS studies have been performed on an octanedithiol (C8-dithiol) SAM using the aforementioned device structure shown in Figure 1(a).[34] Figure 10(a) is the I(V,T) data for this device obtained from 300 to 4.2 K. An Arrhenius plot shown in Figure 10(b) exhibits little temperature dependence, verifying that tunneling is the main transport mechanism for C8-dithiol SAM. This result is in good agreement with the tunneling transport characteristics observed previously. Figure 10(c) shows the room temperature I(V) measurement result. Using a junction area of 51 ± 5 nm in diameter (obtained from statistical studies of the nanopore size with SEM), a current density of $(9.3 \pm 1.8) \times 10^4$ A/cm^2 at 1.0 Volt is calculated. As a comparison, the current density of $(3.1 \pm 1.0) \times 10^4$ A/cm^2 at 1.0 Volt was observed for C8 monothiol SAM. Using the modified Simmons model [Eq. (2)], the transport parameters of $\Phi_B = 1.20 \pm 0.03$ eV and $\alpha = 0.59 \pm 0.01$ ($m^* = 0.34$ m) were obtained for this C8-dithiol SAM.

Figure 10. (a) I(V,T) characteristics of C8 dithiol SAM at selected temperatures (4.2, 50, 100, 150, 200, 250, and 290 K). (b) Arrhenius plot generated from the data in (a), at voltages from 0.1 to 0.5 Volt with 0.05 Volt steps. (c) Measured C8-dithiol I(V) data at room temperature (circular symbols) is compared with calculation (solid curve) using the optimum fitting parameters of $\Phi_B = 1.20$ eV and $\alpha = 0.59$.

Figure 11 shows the IETS spectrum of the same C8-dithiol SAM device obtained at T = 4.2 K. An ac modulation of 8.7 mV (rms value) at a frequency of 503 Hz was applied to the sample to acquire the second harmonic signals. The spectra are stable and repeatable upon successive bias sweeps. The spectrum at 4.2 K is characterized by three pronounced peaks in the 0 to 200 mV region at 33, 133, and 158 mV. From comparison with previously reported infrared (IR), Raman, and high resolution electron energy loss (HREEL) spectra of SAM covered gold surfaces (Table 4), these three peaks are assigned to ν(Au-S), ν(C-C), and $\gamma_w(CH_2)$ modes of a surface bound alkanethiolate.[60-63] The absence of a strong ν(S-H) signal at ~329 mV suggests that most

of the thiol groups have reacted with the gold bottom and top contacts. Peaks are also reproducibly observed at 80, 107 mV, and 186 mV. They correspond to ν(C-S), $\delta_r(CH_2)$, and $\delta_s(CH_2)$ modes. The stretching mode of the CH_2 groups, $\nu(CH_2)$, appears as a shoulder at 357 meV. The peak at 15 mV is due to vibrations from either Si, Au, or δ(C-C-C).[64] We note that all alkanethiolate peaks without exception or omission occur in the spectra. Peaks at 58, 257, 277, and 302, as well as above 375 mV are likely to originate from Si-H and N-H vibrations related to the silicon nitride membrane,[64a,65] which forms the SAM encasement. To the best of our knowledge alkanethiols have no vibrational signatures in these regions. Measurement of the background spectrum of an "empty" nanopore device with only gold contacts to obtain background contributions from Si_3N_4 is hampered by either too low (open circuit) or too high (short circuit) currents in such a device. Similar IETS result has also been obtained using a different test structure recently.[66]

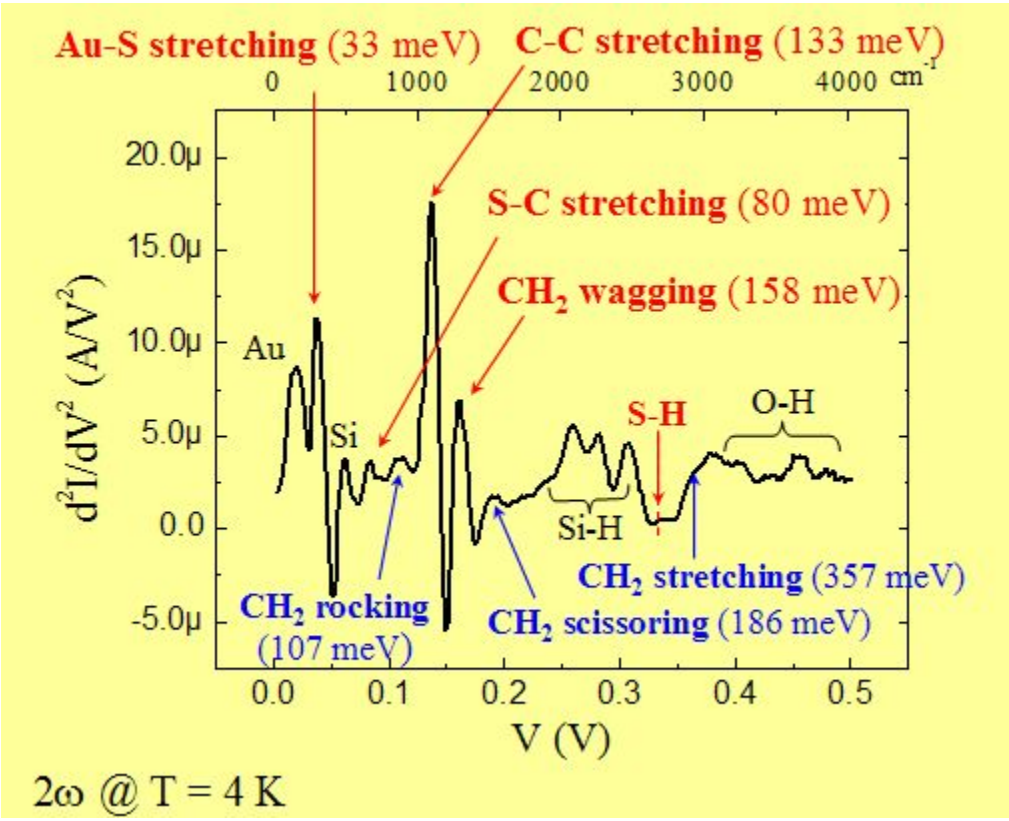

Figure 11. Inelastic electron tunneling spectrum of C8 dithiol SAM obtained from lock-in second harmonic measurement with an ac modulation of 8.7 mV (rms value) at a frequency of 503 Hz (T = 4.2 K). Peaks labeled with Si are most probably background due to the encasing Si_3N_4.

TABLE 4: Summary* of the major vibrational modes of alkanethiolates. Taken from Ref. 60-62.

Modes	Methods	Wavenumber (cm^{-1})	(meV)
ν(Au-S)	HREELS[61]	225	28
ν(C-S)	Raman[60]	641	79

	Raman[60]	706	88
	HREEL[61]	715	89
	IR[62]	720	89
	IR[62]	766	95
	IR[62]	925	115
	HREEL[61]	1050	130
	Raman[60]	1064	132
	Raman[60]	1120	139
	IR[62]	1230	152
	HREELS[61]	1265	157
	IR[62]	1283	159
	IR[62]	1330	165
$\delta_s(CH_2)$	HREELS[61]	1455	180
ν(S-H)	Raman[60]	2575	319
	Raman[60]	2854	354
	HREELS[61]	2860	355
	Raman[60]	2880	357
$\nu_{as}(CH_2)$	Raman[60]	2907	360
	HREELS[61]	2925	363

* There is a vast amount of literature with spectroscopic assignments for alkanethiols. The references given are representative for IR, Raman, and HREELS assignments.

Although there are no selection rules in IETS as there are in IR and Raman spectroscopy, certain selection preferences have been established. According to the IETS theory,[67] molecular vibrations with net dipole moments perpendicular to the interface of the tunneling junction have stronger peak intensities than vibrations with net dipole moments parallel to the interface (for dipoles close to the electrodes). Thus vibrations perpendicular to the electrode interface, i.e., ν(Au-S), ν(C-S), ν(C-C), and $\gamma_w(CH_2)$, dominate the IETS spectrum while modes parallel to the interface, i.e., $\delta_{r,s}(CH_2)$ and $\nu(CH_2)$, are weak, as clearly shown in Figure 11.

In order to verify that the observed spectra are indeed valid IETS data, the peak width broadening was examined as a function of temperature and modulation voltage. IETS was performed with different ac modulations at a fixed temperature, and at different temperatures with a fixed ac modulation. Figure 12(a) shows the modulation dependence of the IETS spectra obtained at 4.2 K, and Figure 12(b) shows the modulation broadening of the C-C stretching mode at 133 meV. The circular symbols are the full widths at half maximum (FWHMs) of the experimental peak at T = 4.2 K with various modulation voltages. A Gaussian distribution function was utilized to obtain a FWHM and the error range.[68] The square symbols are calculated

FWHM values ($W_{theoretical}$) taking into account both a finite temperature effect ($W_{thermal}$ ~ 5.4 k_BT)[36] and a finite voltage modulation effect ($W_{modulation}$ ~ 1.7 V_{ac_rms}).[69] These two broadening contributions add as the squares: $W^2_{theoretical} = W^2_{thermal} + W^2_{modulation}$. The agreement is excellent over most of the modulation range, but we note a saturation of the linewidth at low modulation bias indicating the influence of a non-negligible intrinsic linewidth. Taking into account the known thermal and modulation broadenings, and including the intrinsic linewidth (W_I)[70] as a fitting parameter, the measured peak width (W_{exp}) is given by

$$W_{exp} = \sqrt{W_I^2 + W_{thermal}^2 + W_{modulation}^2} \qquad (6)$$

W_I can be determined by using a nonlinear least squares fit to the ac modulation data (Figure 12) with Eq. (6), giving an intrinsic linewidth of 3.73 ± 0.98 meV for this line. This is shown (with the error range) in Figure 12(b) as a shaded bar, including the thermal contribution.

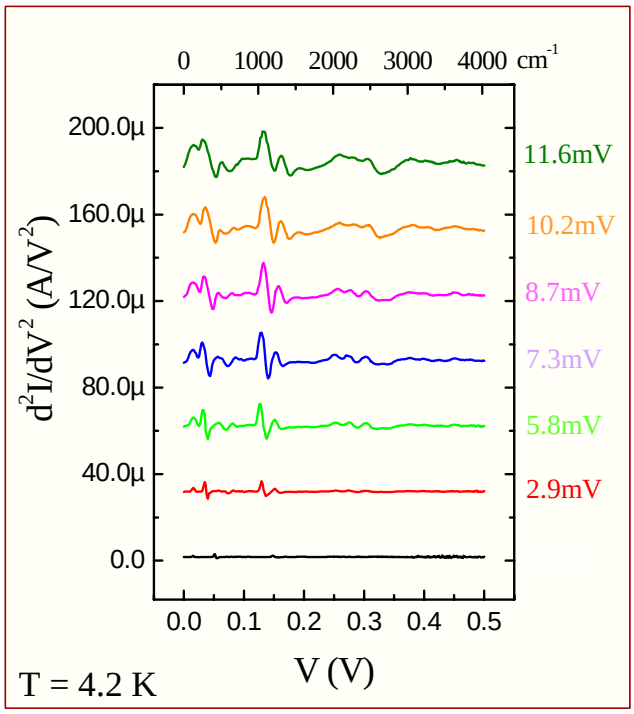

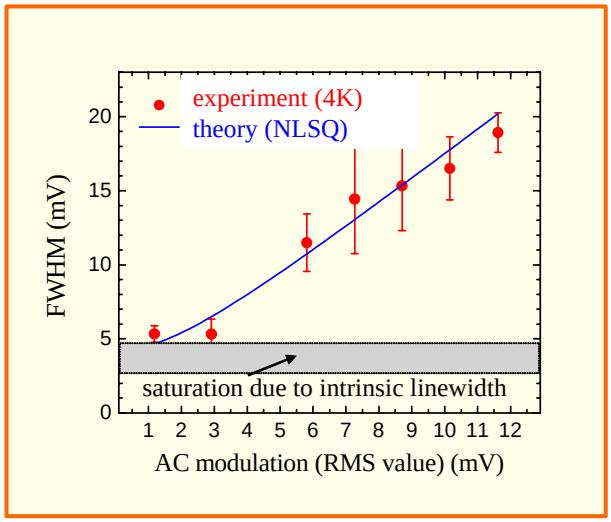

Figure 12. (a) Modulation dependence of IETS spectra obtained at 4.2 K. (b) Line (C-C stretching mode) broadening as a function of ac modulation. The circular symbols are experimental FWHMs and the square symbols are theoretical calculations considering both modulation and thermal contributions. The shaded bar denotes the expected saturation due to the derived intrinsic linewidth (including a 5.4 k_BT thermal contribution) of 3.73 ± 0.98 meV.

We can independently check the thermal broadening of the line at fixed modulation. Figure 13(a) shows the temperature dependence of the IETS spectra obtained with an ac modulation of 8.7 mV (rms value). In Figure 13(b) the circular symbols (and corresponding error bars) are experimental FWHM values of the C-C stretching mode from Figure 13(a), determined by a Gaussian fit (and error of the fit) to the experimental lineshape. For simplicity we have only considered Gaussian lineshapes[68] resulting in increased error bars for the lower temperature range due to an asymmetric lineshape. The square symbols are theoretical calculations considering thermal broadening, modulation broadening, and the intrinsic linewidth determined above. The error ranges of the calculation (due to the intrinsic linewidth error) are approximately the size of the data points. The agreement between theory and experiment is very good, spanning

a temperature range from below (x 0.5) to above (x10) the thermally broadened intrinsic linewidth. This linewidth should be a sensitive test to compare to theoretical models of transmission probabilities.[71]

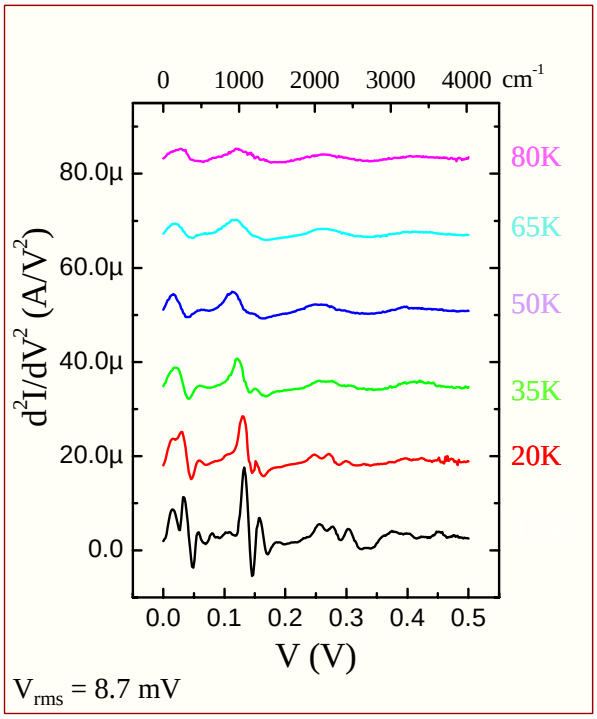

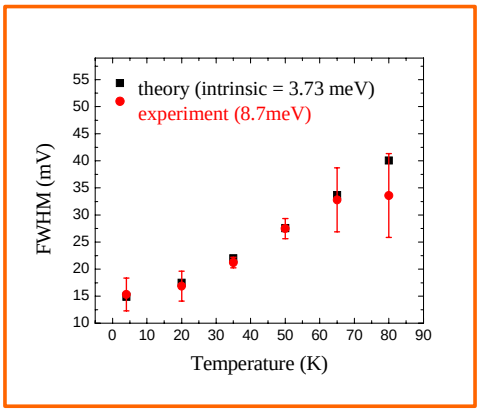

Figure 13. (a) Temperature dependence of IETS spectra obtained at a fixed ac modulation of 8.7 mV (rms value). (b) Line (C-C stretching mode) broadening as a function of temperature. The circular symbols are experimental FWHMs and the square symbols are theoretical calculations considering thermal broadening, modulation broadening, and the intrinsic linewidth. .

Similar intrinsic linewidths have been determined for the Au-S stretching mode (33 meV) and the CH_2 wagging mode (158 meV), and the results are shown in Figure. 14. For the Au-S stretching mode, the deviation of experimental data from calculated values (thermal and modulation width only) is little (Fig. 14(a)), indicating that its intrinsic linewidth is small. A linewidth upper limit of 1.69 meV is determined for this vibrational mode. For the CH_2 wagging mode, a nonlinear least squares fit to Eq. (6) (solid curve in Fig. 14(b)) gave an intrinsic linewidth of 13.5 ± 2.4 meV. The linewidths and their variation throughout the molecule are potentially due to inhomogeneous configuration of the molecular constituents, and a more detailed understanding may give detailed structural information of these device structures.

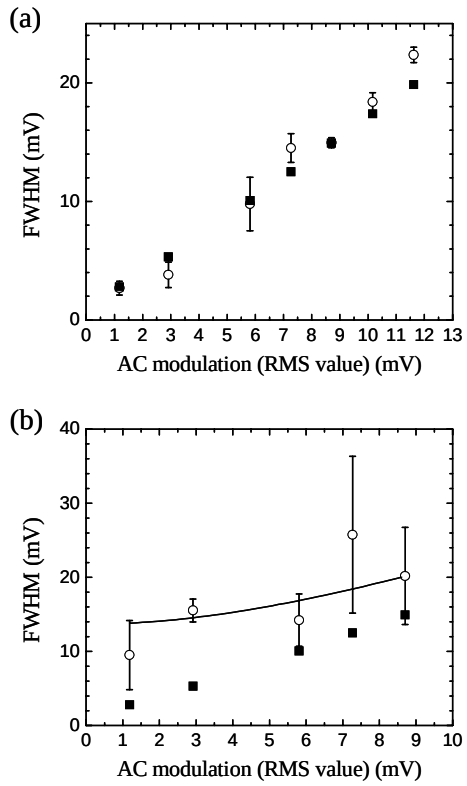

Figure. 14. Line broadenings as function of AC modulation for IETS spectra obtained at 4.2 K for (a) the Au-S stretching mode and (b) the CH_2 wagging mode. The circular symbols are experimental FWHMs and the square symbols are theoretical calculations considering modulation and thermal contributions. Nonlinear least squares fitting to determine intrinsic linewidth is shown as the solid curve in (b). The intrinsic linewidths obtained for the Au-S stretching mode is < 1.69 meV, and for the CH_2 wagging mode is 13.5 ± 2.4 meV.

References

1. Reed, M. A.; Tour, J. M. *Scientific American* **2000**, *June* 86-93.
2. Reed, M. A.; Zhou, C.; Muller, C. J.; Burgin, T. P.; Tour, J. M. *Science* **1997**, *278*, 252-254.
3. Reed, M. A.; Lee, T. Eds. *Molecular Nanoelectronics; American Scientific Publishers*: Stevenson Ranch, 2003.
4. (a) Heath, J. R.; Ratner, M. A. *Physics Today* **2003,** *May* 43-49. (b) Nitzan, A.; Ratner, M. A. *Science* **2003**, *300*, 1384-1389.
5. (a) Chen, Y.; Jung, G.-Y.; Ohlberg, D. A. A.; Li, X.; Stewart, D. R.; Jeppesen, J. O.; Nielsen, K. A.; Stoddart, J. F.; Williams, R. S. *Nanotechnology*, **2003**, *14*, 462-468. (b) Beyond Silicon: Breakthroughs in Molecular Electronics, http://www.hpl.hp.com/ research/qsr/ (Hewlett-Packard Quantum Science Research)
6. (a) Luo, Y.; Collier, C. P.; Jeppesen, J. O.; Nielsen, K. A.; DeIonno, E.; Ho, G.; Perkins, J.; Tseng, H-R.; Yamamoto, T.; Stoddart, J. F.; Heath, J. R. *Chem. Phys. Chem.* **2002,** *3*, 519-525. (b) Collier, C. P.; Mattersteig, G.; Wong, E. W.; Luo, Y.; Beverly, K.; Sampaio, J.; Raymo, F. M.; Stoddart, J. F.; Heath, J. R. *Science* **2000**, *289*, 1172-1175.
7. (a) Stewart, D. R.; Ohlberg, D. A. A.; Beck, P. A.; Chen, Y.; Williams, R. S.; Jeppesen, J. O.; Nielsen, K. A.; Stoddart, J. F. *Nano Lett.* **2004**, *4*, 133-136. (b) Lau, C. N.; Stewart, D. R.; Williams, R. S.; Bockrath, M. *Nano Lett.* **2004**, *4*, 569-572.
8. Lee, T.; Wang, W.; Klemic, J. F.; Zhang, J. J.; Su, J.; Reed, M. A. *J. Phys. Chem. B* **2004**, 108, 8742-8750.
9. Ulman, A. *An Introduction to Ultrathin Organic Films from Langmuir-Blodgett to Self-Assembly*; Academic Press: Boston, 1991.
10. Poirier, G. E. *Chem. Rev.* **1997**, *97*, 1117-1127.
11. Ratner, M, A,; Davis, B.; Kemp, M.; Mujica, V.; Roitberg, A.; Yaliraki, S. in *Molecular Electronics: Science and Technology*, *The Annals of the New York Academy of Sciences*, Aviram, A.; Ratner, M. Eds.; The New York Academy of Sciences: Vol. 852, New York, 1998.
12. Although the HOMO-LUMO gap of alkyl chain type molecules has been reported (see ref 13), there is no experimental data on the HOMO-LUMO gap for Au/alkanethiol SAM/Au system. 8 eV is commonly used as HOMO-LUMO gap of alkanethiol.
13. (a) Boulas, C.; Davidovits, J. V.; Rondelez, F.; Vuillaume, D. *Phys. Rev. Lett.* **1996**, *76*, 4797-4800. (b) Fujihira, M.; Inokuchi, H. *Chem. Phys. Lett.* **1972**, *17*, 554-556. (c) Lias, S. G.; Bartmess, J. E.; Liebman, J. F.; Holmes, J. L.; Levin, R. D.; Mallard, W. G. *Gas-Phase Ion and Neutral Thermochemistry*, *J. Phys. Chem. Ref. Data*, **1998**, *17(1)*, 24. (d) Yang, H-H; McCreery, R. L. Anal. Chem. **1999**, 71, 4081.
14. Walczak, M. W.; Chung, C.; Stole, S. M.; Widrig, C. A.; Porter, M. D. *J. Am. Chem. Soc.* **1991**, *113*, 2370-2378.
15. Nuzzo, R. G.; Zegarski, B. R.; Dubois, L. H. *J. Am. Chem. Soc.* **1987**, *109*, 733-740.
16. Widrig, C. A.; Chung, C.; Porter, M. D. *J. Electroanal. Chem.* **1991**, *310*, 335-359.
17. Poirier, G. E.; Tarlov, M. J. *Langmuir* **1994**, *10*, 2853-2856.
18. Porter, M. D.; Bright, T. B.; Allara, D. L.; Chidsey, C. E. D. *J. Am. Chem. Soc.* **1987**, *109*, 3559-3568.
19. Bumm, L. A.; Arnold, J. J.; Dunbar, T. D.; Allara, D. L.; Weiss, P. S. *J. Phys. Chem.* B **1999**, *103*, 8122-8127.
20. Xu, B.; Tao, N. J. *Science* **2003**, *301*, 1221-1223.
21. Wold, D. J.; Frisbie, C. D. *J. Am. Chem. Soc.* **2001**, *123*, 5549-5556.
22. Wold, D. J.; Haag, R.; Rampi, M. A.; Frisbie, C. D. *J. Phys. Chem. B* **2002**, *106*, 2813-2816.
23. Cui, X. D.; Zarate, X.; Tomfohr, J.; Sankey, O. F.; Primak, A.; Moore, A. L.; Moore, T. A.; Gust, D.; Harris, G.; Lindsay, S. M. *Nanotechnology* **2002**, *13*, 5-14.
24. Cui, X. D.; Primak, A.; Zarate, X.; Tomfohr, J.; Sankey, O. F.; Moore, A. L.; Moore, T. A.; Gust, D.; Nagahara, L. A.; Lindsay, S. M. *J. Phys. Chem. B* **2002**, *106*, 8609-8614.

25. Holmlin, R.; Haag, R.; Chabinyc, M. L.; Ismagilov, R. F.; Cohen, A. E.; Terfort, A. Rampi, M. A.; Whitesides, G. M. *J. Am. Chem. Soc.* **2001**, *123*, 5075-5085.
26. Rampi, M. A.; Whitesides, G. M. *Chem. Phys.* **2002**, *281*, 373-391.
27. Slowinski, K.; Fong, H. K. Y.; Majda, M. *J. Am. Chem. Soc.* **1999**, *121*, 7257-7261.
28. York, R. L.; Nguyen, P. T.; Slowinski, K. *J. Am. Chem. Soc.* **2003**, *125*, 5948-5953.
29. Kushmerick, J. G.; Holt, D. B.; Pollack, S. K.; Ratner, M. A.; Yang, J. C.; Schull, T. L.; Naciri, J.; Moore, M. H.; Shashidhar, R. *J. Am. Chem. Soc.* **2002**, *124*, 10654-10655.
30. Smalley, J. F.; Feldberg, S. W.; Chidsey, C. E. D.; Linford, M. R.; Newton, M. D.; Liu, Y. *J. Phys. Chem.* **1995**, *99*, 13141-13149.
31. Weber, K.; Hockett, L.; Creager, S. *J. Phys. Chem. B* **1997**, *101*, 8286-8291.
32. Slowinski, K.; Chamberlain, R. V.; Miller, C. J.; Majda, M. *J. Am. Chem. Soc.* **1997**, *119*, 11910-11919.
33. Wang, W.; Lee, T.; Reed, M. A. *Phys. Rev. B* **2003**, *68*, 035416.
34. Wang, W.; Lee, T.; Kretzschmar, I.; Reed, M. A. *Nano Lett.* **2004**, *4*, 643-646.
35. Jaklevic, R. C.; Lambe, J. *Phys. Rev. Lett.* **1966**, *17*, 1139-1140.
36. Lambe, J.; Jaklevic, R. C. *Phys. Rev.* **1968**, *165*, 821-832.
37. Adkins, C. J.; Phillips, W. A. *J. Phys. C: Solid State Phys.* **1985**, *18*, 1313-1346.
38. Hansma, P.K., Ed. *Tunneling Spectroscopy: Capabilities, Applications, and New Techniques*; Plenum: New York, 1982.
39. Stipe, B. C.; Rezaei, M. A.; Ho, W. *Science* **1998,** *280*, 1732-1735.
40. Zhou, C.; Deshpande, M. R.; Reed, M. A.; Jones II, L.; Tour, J. M. *Appl. Phys. Lett.* **1997**, *71*, 611-613.
41. (a) Chen, J.; Reed, M. A.; Rawlett, A. M.; Tour, J. M. *Science* **1999**, *286*, 1550-1552. (b) Chen, J.; Calvet, L. C.; Reed, M. A.; Carr, D. W.; Grubisha, D. S.; Bennett, D. W. *Chem. Phys. Lett.* **1999**, *313*, 741-748.
42. Ralls, K. S.; Buhrman, R. A.; Tiberio, R. C. *Appl. Phys. Lett.* **1989**, *55*, 2459-2461.
43. Ethanol and alkane molecules were purchased from Sigma-Aldrich.
44. Metzger, R. M.; Chen, B.; Ho1pfner, U.; Lakshmikantham, M. V.; Vuillaume, D.; Kawai, T.; Wu, X.; Tachibana, H.; Hughes, T. V.; Sakurai, H.; Baldwin, J. W.; Hosch, C.; Cava, M. P.; Brehmer, L.; Ashwell, G. J. *J. Am. Chem. Soc.* **1997**, *119*, 10455-10466.
45. Horowitz, P.; Hill, W. *The Art of Electronics*; Cambridge University Press: New York, 1989.
46. Sze, S. M. *Physics of Semiconductor Devices*; Wiley: New York, 1981.
47. (a) Thurstans, R. E.; Oxley, D. P. *J. Phys. D: Appl. Phys.* **2002**, *35*, 802-809. (b) Simmons, J. G.; Verderber, R. R. *Prof. Roy. Soc. A.* **1967**, *301*, 77-102. (c) Dearnaley, G.; Stoneham, A. M.; Morgan, D. V. *Rep. Prog. Phys.* **1970**, *33*, 1129-1191.
48. (a) Mann, B.; Kuhn, H. *J. Appl. Phys.* **1971**, *42*, 4398-4405. (b) Polymeropoulos, E. E.; Sagiv, J. *J. Chem. Phys.* **1978**, *69*, 1836-1847.
49. Fan, F. F.; Yang, J.; Cai, L.; Price, D. W.; Dirk, S. M.; Kosynkin, D. V.; Yao, Y.; Rawlett, A. M.; Tour, J. M.; Bard, A. J. *J. Am. Chem. Soc.* **2002**, *124*, 5550-5560.
50. Franz, W. in *Handbuch der Physik*, edited by Flugge, S; Springer-Verlag: Berlin, 1956, Vol. 17, p. 155.
51. (a) Lewicki, G.; Mead, C. A. *Phys. Rev. Lett.* **1966**, *16*, 939-941. (b) Stratton, R.; Lewicki, G.; Mead, C. A. *J. Phys. Chem. Solids.* **1966**, *27*, 1599-1604. (c) Parker, G. H.; Mead, C. A. *Phys. Rev. Lett.* **1968**, *21*, 605-607.
52. Brar, B.; Wilk, G. D.; Seabaugh, A. C. *Appl. Phys. Lett.* **1996**, *69*, 2728-2730.
53. Joachim, C.; Magoga, M. *Chem. Phys.* **2002**, *281*, 347-352.
54. Simmons, J. G. *J. Appl. Phys.* **1963**, *34*, 1793-1803.
55. (a) Simmons, J. G. *J. Phys. D* **1971**, *4*, 613-657. (b) Maserjian, J.; Petersson, G. P. *Appl. Phys. Lett.* **1974**, *25*, 50-52.
56. Tomfohr, J. K.; Sankey, O. F. *Phys. Rev. B* **2002**, *65*, 245105.

57. (a) Yamamoto, H.; Waldeck, D. H. *J. Phys. Chem. B* **2002**, *106*, 7469-7473. (b) Napper, A. M.; Liu, Haiying.; Waldeck, D. H. *J. Phys. Chem. B* **2001**, *105*, 7699-7707.
58. Kaun, C.-C.; Guo, H. *Nano Lett.* **2003**, *3*, 1521-1525.
59. Piccinin, S.; Selloni, A.; Scandolo, S.; Car, R.; Scoles, G. *J. Chem. Phys*. **2003**, *119*, 6729-6735.
60. Bryant, M. A.; Pemberton, J. E. *J. Am. Chem. Soc.* **1991**, *113*, 8284-8293.
61. Kato, H. S.; Noh, J.; Hara, M.; Kawai, M. *J. Phys. Chem. B* **2002**, *106*, 9655-9658.
62. Castiglioni, C.; Gussoni, M.; Zerbi, G. J. *Chem. Phys.* **1991**, *95*, 7144-7149.
63. The symbols δ, γ, and ν denote in-plane rocking (r) and scissoring (s), out-of-plane wagging (w) and twisting (t), and stretching modes, respectively.
64. a) Molinari, M.; Rinnert, H.; Vergnat, M.; Weisbecker, P. *Mat. Sci. Eng. B* **2003**, 101, 186. b) Bogdanoff, P. D.; Fultz, B.; Rosenkranz, S. *Phys. Rev. B* **1999**, *60*, 3976-3981. c) Mazur, U.; Hipps, K. W. *J. Phys. Chem.* **1982**, *86*, 2854-2860.
65. a) Mazur, U.; Hipps, K. W. *J. Phys. Chem.* **1981**, *85*, 2244-2249. b) Kurata, H.; Hirose, M.; Osaka, Y. *Jap. J. Appl. Phys*. **1981**, *20*, L811.
66. Kushmerick, J. G.; Lazorcik, J.; Patterson, C. H.; Shashidhar, R.; Seferos, D. S.; Bazan, G. C. *Nano Lett*. **2004**, *4*, 639-642.
67. Kirtley, J.; Hall, J. T. *Phys. Rev. B* **1980**, *22*, 848-856.
68. Lauhon, I. J.; Ho, W. *Phys. Rev. B* **1999**, *60*, R8525-R8528.
69. Klein, J.; Léger, A.; Belin, M.; Défourneau, D.; Sangster, M. J. L. *Phys. Rev. B* **1973**, *7*, 2336-2348.
70. Lauhon, L. J.; Ho, W. *Rev. Sci. Instrum*. **2001,** *72*, 216-223.
71. Kastner, M. A. *Physics Today* **1993,** *January* 24-31.
72. Aviram, A.; Ratner, M. Eds. *Molecular Electronics: Science and Technology, The Annals of the New York Academy of Sciences*; The New York Academy of Sciences: Vol. 852, New York, 1998.
73. Reimers, J; Picconatto, C; Ellenbogen, J; Shashidhar, R, *Molecular Electronics III, The Annals of the New York Academy of Sciences*; The New York Academy of Sciences: Vol. 1006, New York, 2003.

Personnel supported

Prof. Mark Reed, PI
Dr. Guosheng Cheng (research scientist)
Dr. James Klemic (research scientist)

Publications

Book chapters:

1. W. Wang, T. Lee, and M.A. Reed, "Electronic Transport Through Self-Assembled Monolayers", *Nanoscale Assembly*, edited by Wilhelm Huck, (Kluwer Academic/Plenum Publishers, 2005).
2. W. Wang, T. Lee, and M.A. Reed, "Intrinsic Electronic Conduction Mechanisms in Self-Assembled Monolayers", *Introducing Molecular Electronics*, Proceedings of the Dresden ADMOL Conference, *Lect. Notes Phys.* **680**, 275-300 (2005).

Journal articles

1. W. Wang, T. Lee, I. Kretzschmar, and M.A. Reed, “Inelastic Electron Tunneling Spectroscopy of Alkanedithiol Self-Assembled Monolayers”, *Nano Lett.* **4**, 643 (2004).
2. Reed, M.A., “Molecular Electronics – Back under control”, Nature Materials **3**, 286 (2004).
3. Lee, T.; Wang, W.; Klemic, J. F.; Zhang, J. J.; Su, J.; Reed, M. A., “Comparison of Electronic Transport Characterization Methods for Alkanethiol Self-Assembled Monolayers”, *J. Phys. Chem. B.* **108**, 8742 (2004).
4. W. Wang, T. Lee, and M.A. Reed, “Elastic and Inelastic Electron Tunneling in Alkane Self-Assembled Monolayers”, *J. Phys. Chem. B.* **108**, 18398 (2004). **(cover, feature article)**.
5. T. Lee, W. Wang, and M. A. Reed, “Intrinsic Electronic Transport through Alkanedithiol Self-Assembled Monolayer”, *J. Jour. Appl. Phys*. **44**, 523 (2005).
6. W. Wang, T. Lee, and M.A. Reed, “Electron Tunneling in Alkane Self-Assembled Monolayers”, *Rep. Prog. Phys.* **68**, 523 (2005).
7. T. Lee, W. Wang, J. J. Zhang, J. Su, J. F. Klemic, and M. A. Reed, “Cross-platform characterization of electron tunneling in molecular self-assembled monolayers”, *Curr. Appl. Phys.* **5**, 213 (2005).
8. W. Wang, T. Lee, and M.A. Reed, “Electronic Transport in Molecular Self-Assembled Monolayer Devices”, *Proc. IEEE* **93** (2005).

Interactions/Transitions

Numerous talk and seminars. No consultations or transitions

New discoveries, patents

none